Bose-Einstein Condensation of Magnons and Spin Superfluidity in the Polar Phase of ^{3}He

S. Autti,[1,*] V. V. Dmitriev,[2] J. T. Mäkinen,[1] J. Rysti,[1] A. A. Soldatov,[2,3] G. E. Volovik,[1,4] A. N. Yudin,[2] and V. B. Eltsov[1]

[1]*Department of Applied Physics, Aalto University, P.O. Box 15100, FI-00076 AALTO, Finland*
[2]*P. L. Kapitza Institute for Physical Problems of RAS, 119334 Moscow, Russia*
[3]*Moscow Institute of Physics and Technology, 141700 Dolgoprudny, Russia*
[4]*Landau Institute for Theoretical Physics, 142432 Chernogolovka, Russia*

(Received 13 November 2017; revised manuscript received 9 February 2018; published 12 July 2018)

The polar phase of ^{3}He, which is topological spin-triplet superfluid with the Dirac nodal line in the spectrum of Bogoliubov quasiparticles, has been recently stabilized in a nanoconfined geometry. We pump magnetic excitations (magnons) into the sample of polar phase and observe how they form a Bose-Einstein condensate, revealed by coherent precession of the magnetization of the sample. Spin superfluidity, which supports this coherence, is associated with the spontaneous breaking of U(1) symmetry by the phase of precession. We observe the corresponding Nambu-Goldstone boson and measure its mass emerging when applied rf field violates the U(1) symmetry explicitly. We suggest that the magnon BEC in the polar phase is a powerful probe for topological objects such as vortices and solitons and topological nodes in the fermionic spectrum.

DOI: 10.1103/PhysRevLett.121.025303

Introduction.—The phenomenon of Bose-Einstein condensation, originally suggested for real particles and observed in ultracold gases, has been extended in recent experimental and theoretical works to systems of bosonic quasiparticles, including collective modes. Examples are longitudinal electric modes [1], phonons [2], excitons [3], exciton-polaritons [4], photons [5], rotons [6], and magnons [7–17]. In these systems, quasiparticles are externally pumped, but they are sufficiently long-lived, so that their number N is quasiconserved. As a result, the chemical potential $\mu = dE/dN$ is nonzero during the lifetime of the condensate.

The Bose-Einstein condensate (BEC) of magnons was discovered in the B phase of ^{3}He [7]. In this spin-triplet superfluid, magnons are quanta of transverse spin waves, associated with the precessing spin of ^{3}He nuclei. Magnon condensation results in the spontaneous coherence of the precession, which produces a characteristic signal in nuclear magnetic resonance (NMR) experiments [7]. In the experiment, magnons, carrying spin $-\hbar$, are pumped using a radio-frequency (rf) pulse, which deflects magnetization $\mathbf{M}$ (or spin $\mathbf{S}$) from the equilibrium direction along the magnetic field $\mathbf{H}\|\hat{\mathbf{z}}$. Alternatively, magnons can be continuously replenished with a small rf field $\mathbf{H}_{\rm rf}\perp\mathbf{H}$ to compensate for magnetic relaxation [8].

The coherent precession $(S_x + iS_y) \propto e^{i(\omega t+\phi)}$ is characterized by a common frequency ω and definite phase ϕ. The formation of the coherent phase ϕ across the whole sample reveals the spontaneously broken SO(2) spin rotation symmetry. In the language of the magnon BEC, this corresponds to the breaking of the U(1) symmetry. This symmetry characterizes the (approximate) conservation law for the number of magnons: $N_M = \int dV(S - S_z)/\hbar$, while the chemical potential determines the frequency of precession $\mu = dE/dN_M = \hbar\omega$.

Spontaneous breaking of U(1) symmetry is linked to the superfluid phase transition. In the case of magnon BEC, this is spin superfluidity. Experiments in ^{3}He-B demonstrated various phenomena that accompany the spin superfluidity, such as ac and dc Josephson effects, spin supercurrents, and phase-slip processes [18–20]. Another important marker of the spontaneous U(1) symmetry breaking is the appearance of the Nambu-Goldstone (NG) mode (which is a phonon in a usual superfluid) [21,22]. For magnon condensates in ^{3}He-B, such a mode was indeed experimentally found [23].

Besides demonstrating the fascinating phenomenon of spin superfluidity, the magnon BEC in ^{3}He-B proved to be a sensitive probe for topological structures of the order parameter, like quantized vortices and their dynamics [24–28], for fermionic quasiparticles [29] and for bosonic collective modes [30]. This coherent probe can be made local by trapping magnons in magnetic and textural traps [10,12]. For a sufficiently large number of pumped magnons, the condensate deforms the trap [13], which leads to the formation of a self-trapped magnon BEC [31]. The latter is an exact implementation of the Q balls studied in relativistic quantum field theories, which shows that magnon BEC can also be used for quantum simulations.

We expect magnon BEC to also provide deep insight into other topological superfluids. The coherent precession of magnetization was predicted to exist in superfluid ^{3}He-A [32], and its observation was reported in the A-like phase in

silica aerogel [33]. Here, we demonstrate magnon BEC in the recently discovered polar phase of superfluid ^{3}He. We observe the coherent precession of magnetization using NMR techniques. We also measure the collective NG mode of the condensate as a function of temperature, rf excitation amplitude, precession frequency, and magnetic field orientation.

Polar phase.—The polar phase is realized in liquid ^{3}He confined within Nafen [34], a commercially produced nanostructured material that consists of nearly parallel Al_2O_3 strands [35]. The order parameter in the polar phase is

$$A_{\nu j} = \Delta_0 e^{i\varphi} \hat{d}_\nu \hat{m}_j, \tag{1}$$

where Δ_0 is the gap parameter, $e^{i\varphi}$ is the phase factor, and $\hat{\mathbf{d}}$ and $\hat{\mathbf{m}}$ are the unit vectors of spin and orbital anisotropy, respectively. In Nafen, $\hat{\mathbf{m}}$ is locked parallel to the strands [36]. The polar phase is a Dirac superfluid that belongs to the same class of topological matter as Dirac nodal-line semimetals [37–39]. As distinct from the fully gapped ^{3}He-B and from ^{3}He-A with Weyl nodes, the gap in the polar phase has a line of zeros in the plane normal to $\hat{\mathbf{m}}$.

Experiment.—The Nafen sample is a cube with a side of 4 mm. It has a porosity of 94% and a density of 0.243 g/cm^3. The strands are 9 nm in diameter, and they are separated on average by 35 nm [35]. Experiments are performed at pressures of 6.9–7.1 bar using pulsed and continuous-wave (cw) NMR in a magnetic field of 11.2 mT, corresponding to the NMR frequency of 362.8 kHz. The static magnetic field $\mathbf{H}$ can be applied at an arbitrary angle λ with respect to $\hat{\mathbf{m}}$. The sample is cooled down in the ROTA nuclear demagnetization refrigerator [29], and the temperature is measured by a quartz tuning fork [40]. The fork is calibrated against the NMR spectra measured in the linear regime using the known Leggett frequency in bulk ^{3}He-B [41,42] and in the polar phase [34,43]. To avoid the formation of paramagnetic solid ^{3}He on the surfaces and to stabilize the polar phase, the sample is preplated by about 2.5 atomic layers of ^{4}He [44]. The magnitude of the rf magnetic field $H_{\rm rf} \ll H$ is calibrated with a $\pi/2$ NMR pulse in normal ^{3}He.

Coherent precession.—The liquid ^{3}He in our sample becomes superfluid at $0.95T_c$, where T_c is the superfluid transition temperature in bulk ^{3}He. In the temperature range of our measurements, down to $0.3T_c$, only the polar phase is observed. In the polar phase, the NMR frequency is given by [36]

$$\omega = \omega_L + \frac{\Omega_P^2}{2\omega_L}\left[\cos\beta - \frac{\sin^2\lambda}{4}(5\cos\beta - 1)\right]. \tag{2}$$

Here, β is the deflection angle of the magnetization from the magnetic field direction (Fig. 1), Ω_P is the Leggett frequency in the polar phase, $\omega_L = \gamma H$ is the Larmor frequency, and $\gamma = 2.04 \times 10^8$ s^{-1} T^{-1} is the absolute value

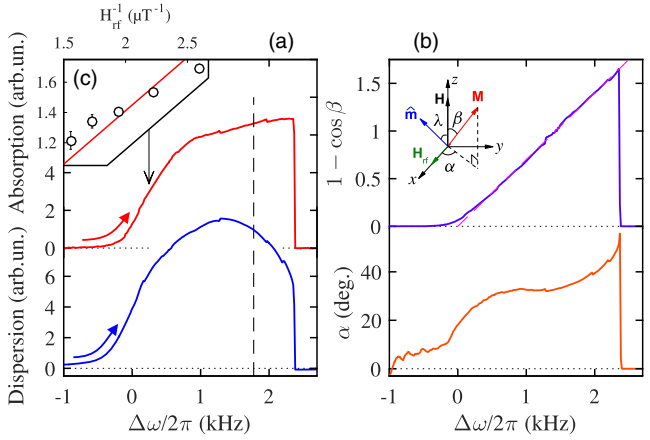

FIG. 1. Creation of coherently precessing state in the polar phase of ^{3}He using cw NMR. (a) Absorption and dispersion signals recorded on a sweeping down magnetic field H with $H_{\rm rf} = 0.32$ μT at $T = 0.41T_c$, $P = 6.9$ bar, and $\lambda = 90°$. On the horizontal axis, the frequency shift $\omega_{\rm rf} - \gamma H$ is shown. (b) The tipping angle β and the phase of precession α of magnetization $\mathbf{M}$ are determined from the records in the panel (a). Definition of the angles is given in the inset. Magnetization $\mathbf{M}$ is in a rotating frame of precession. Absorption and dispersion signals are proportional to $M_y = M\sin\beta\sin\alpha$ and $M_x = M\sin\beta\cos\alpha$, respectively. The relation between $\Delta\omega$ and $\cos\beta$ is linear (dashed line) in accordance with Eq. (2). (c) Cw NMR absorption versus $H_{\rm rf}^{-1}$ at the fixed $\Delta\omega/(2\pi) = 246$ Hz at $T = 0.43T_c$, $P = 7.1$ bar, and $\lambda = 90°$. The solid line is a linear fit through zero.

of the gyromagnetic ratio of ^{3}He. Most of our experiments are performed in a transverse magnetic field ($\lambda = 90°$). In this case, in cw NMR, where $\cos\beta \approx 1$, the frequency shift $\Delta\omega = \omega - \omega_L$ equals zero.

Coherent precession of magnetization is stable only if $d\omega/d(\cos\beta) < 0$ [45], which corresponds to the repulsion between magnons, $d\mu/dn_M > 0$. Here, the magnon density is $n_M = (S - S_z)/\hbar = (\chi H/\gamma\hbar)(1 - \cos\beta)$, where χ is the magnetic susceptibility. In the polar phase, the stability condition is satisfied when $|\tan\lambda| > 2$, while the tipping angle of magnetization β can be arbitrary. The critical magnetic field direction is $\lambda_c = \arctan 2 \approx 63.4°$. In the stable region, superfluid spin currents act to maintain the coherent precession by redistributing magnetization (and n_M) across the sample in such a way that the precession frequency ω in Eq. (2) remains uniform even if ω_L, λ and Ω_P have spatial dependence due to field inhomogeneity and disorder within Nafen.

The coherent precession is observed in the cw NMR experiment as follows: We initially apply the magnetic field, $H > \omega_{\rm rf}/\gamma$, where $\omega_{\rm rf}$ is a fixed frequency of rf excitation. Then, we gradually decrease H. While the resonance condition is approached, magnetization deflects and β increases, which results in a positive frequency shift of precession $\Delta\omega > 0$ according to Eq. (2). When ω_L becomes smaller than $\omega_{\rm rf}$ during the field sweep, this frequency shift may compensate the difference, and ω in

Eq. (2) becomes locked to $\omega_{\rm rf}$ despite the fact that ω_L is changing. For this locking to occur, the rf excitation should be large enough to compensate the magnetic relaxation. An example of the NMR signals measured in this way is shown in Fig. 1(a). As one can see in Fig. 1(b), $\mathbf{M}$ can be deflected by more than 90°. The dissipation grows with increasing β, and eventually, the precessing state collapses, in this case at $\beta \approx 130°$.

The coherent nature of the created state is revealed during its decay, Fig. 2. After switching off the rf pumping, magnetic relaxation results in a decrease of N_M, and the frequency of precession ω gradually decreases according to Eq. (2). The recorded signal is strikingly longer than the decay of incoherent precession in normal ^{3}He. The latter time is determined by dephasing, owing to the magnetic field inhomogeneity $\Delta H/H \approx 8 \times 10^{-4}$. In coherent precession, the dephasing is absent, and the decay rate of magnon BEC is set by the energy dissipation, which leads to matching relaxation time scales for the frequency and the amplitude of precession, seen in Fig. 2. The relaxation can be independently estimated from the absorption M_y in the cw NMR spectrum, $\dot{E} = \gamma H_{\rm rf} H M_y$. In a driven coherently precessing state, the profile of magnetization and thus $\dot{E}$ is determined by the frequency shift $\Delta\omega$ of the drive from the Larmor. The proportionality $M_y \propto H_{\rm rf}^{-1}$ at a fixed $\Delta\omega$ is indeed seen in Fig. 1(c). Expressing energy of the magnon BEC via β, one obtains an energy balance in the form $\dot{\beta} = -\gamma H_{\rm rf} \sin\alpha(\beta)$, where $H_{\rm rf}$ and dependence $\alpha(\beta)$ refer to cw NMR spectra in Fig. 1. Solving the equation and converting β to corresponding frequency using Fig. 1(b), we obtain a solid line in Fig. 2, which is in a reasonable agreement with the measured $\Delta\omega$.

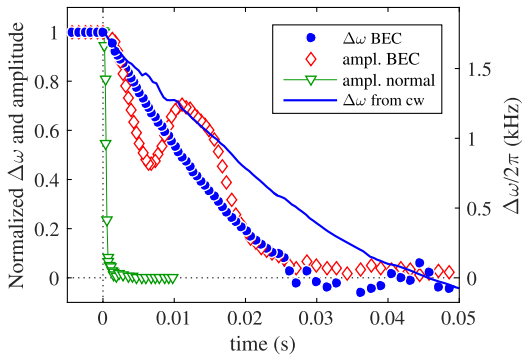

FIG. 2. Long-living coherent precession is demonstrated by a free induction decay (FID) signal recorded after turning off at $t = 0$ the rf excitation at the frequency shift marked by the dashed line in Fig. 1(a). Frequency (filled circle) and amplitude (diamond) are obtained by fitting a sine wave to short sections of the raw signal. Oscillations on the amplitude are due to the excitation of the NG mode. Linear extrapolation of $\cos\beta$ to 1 in Fig. 1(b) is taken as zero frequency. The solid line shows the expected time dependence of $\Delta\omega$ calculated from cw NMR data in Fig. 1, assuming relaxation only due to magnon loss. Much faster dephasing time for incoherent precession is demonstrated by a FID signal measured in normal ^{3}He (inverted triangle).

Magnon BEC, in the polar phase, forms in the presence of strong inhomogeneity, provided by the confining Nafen matrix, which is an important difference from the well-studied case of bulk ^{3}He-B. While the frequency ω remains uniform across the whole volume of the polar phase, an inhomogeneous β profile develops according to Eq. (2). During the decay, gradients of α build up to drive spin currents, which maintain the required profile of β (or magnon density n_M) in the presence of relaxation. As a result, (i) relaxation during decay increases compared to cw NMR (owing to dissipative spin transport in parallel to spin supercurrents). This is clearly seen in Fig. 2. (ii) The measured signal amplitude $M_y = \chi H \int dV \sin\beta \sin\alpha$ cannot be quantitatively compared to expectations in the absence of knowledge about the $\alpha(\mathbf{r})$ profile. (iii) Close to the end of the decay, where the total number of magnons N_M becomes small, the required profile of n_M cannot be maintained in the whole sample volume, and the region of coherent precession contracts to the deepest well in the background potential, which decreases the relaxation rate similar to Q balls in ^{3}He-B [10,12,31].

Nambu-Goldstone mode.—The spin rigidity of magnon BEC allows for low-frequency oscillations of the magnetization on the background of the coherent precession. This oscillating mode has a relativistic spectrum

$$\Omega^2 = \mathcal{M}^2 + c^2 k^2, \tag{3}$$

where Ω is the frequency, k is the wave vector of the oscillations, and c is the propagation velocity. For a pure NG mode resulting from spontaneous U(1) symmetry breaking in magnon BEC, the mass (or gap) $\mathcal{M}$ is zero. If magnon BEC is supported by pumping, like in our cw NMR experiments, then explicit breaking of the U(1) symmetry by rf field opens a gap in the spectrum, and the mode becomes pseudo-Nambu-Goldstone. For magnon condensates in ^{3}He-B, the mass of the pseudo-NG mode was measured in Refs. [46,47]. In the polar phase, the mass is given by [48]

$$\mathcal{M}^2 = \frac{\Omega_P^2}{8} \frac{H_{\rm rf}}{H} (1 - 5\cos^2\lambda) \sin\beta \cos\alpha, \tag{4}$$

where the factor $\cos\alpha$ accounts for the fact that oscillations of the phase of precession occur around nonzero α, owing to the dissipation.

The boundary conditions in our sample (vanishing spin current through the boundary) allow for spatially uniform oscillations with $k = 0$ and frequency $\Omega = \mathcal{M}$. In the experiment, this mode can be excited by the driving phase of the precession α out of equilibrium, e.g., by changing (during precession) the static magnetic field or phase (or amplitude) of the rf drive. We have used an alternating

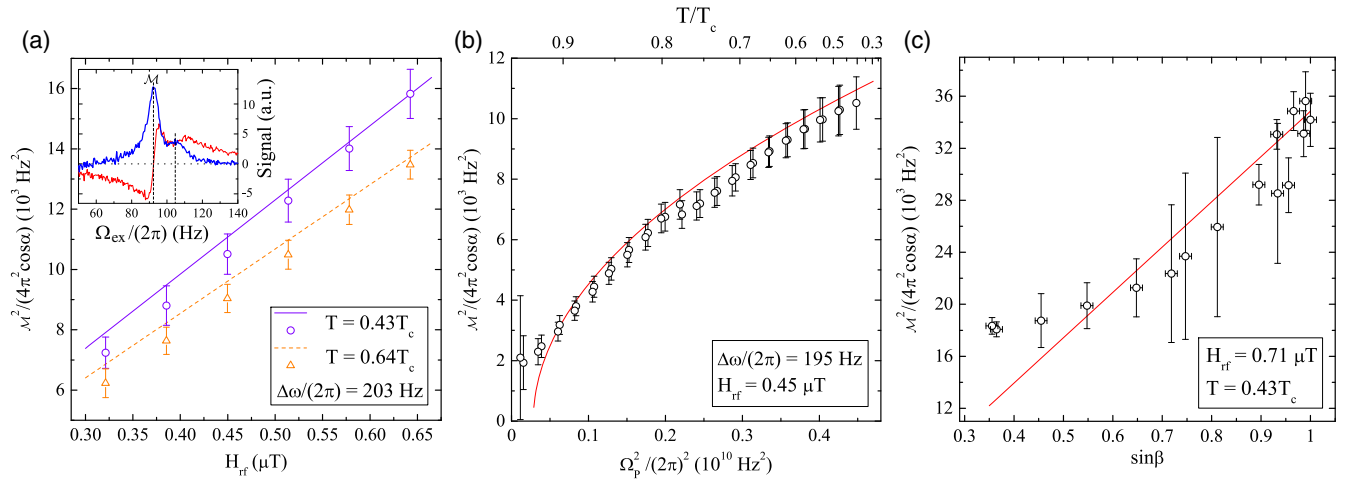

FIG. 3. The mass $\mathcal{M}$ of the pseudo-Nambu-Goldstone mode in magnon BEC supported by cw NMR in the polar phase of ^{3}He as a function of $H_{\rm rf}$ (a), Ω_P (b), and $\sin\beta$ (c) at $P = 7.1$ bar and $\lambda = 90°$. Symbols are experimental data, curves are theoretical predictions of Eq. (4) without fitting. Inset to panel (a) shows an example of excitation spectrum of magnon BEC measured as described in the text with 3×10^{-6} relative peak-to-peak variation of the static field. A set of peaks (marked by dashed lines) is seen and $\mathcal{M}$ is given by the frequency of the largest peak, while the error bar is determined as the peak width. The Leggett frequency $\Omega_P(T)$ is determined from cw NMR spectra at $\lambda = 0$. Values of $\cos\alpha$, which depend on $H_{\rm rf}$ and $\Delta\omega$, are calculated from absorption and dispersion signals, while $\sin\beta$ is determined from Eq. (2).

(with frequency $\Omega_{\rm ex}$) field gradient along $\mathbf{H}$. Oscillations of α result in periodic variation of the NMR signal. The absorption or dispersion signal is detected by a lock-in amplifier at frequency ω, and the output is wired to the input of a second lock-in tuned to the frequency of the gradient modulation. Using the second lock-in, we record secondary absorption and dispersion signals as a function of $\Omega_{\rm ex}$, as illustrated in the inset in Fig. 3(a). The main peak is fitted by a Lorentzian to obtain the resonance frequency of the pseudo-NG mode $\mathcal{M}$. The secondary spectrum also shows other peaks, probably corresponding to standing waves of a pseudo-NG mode with finite k, but a detailed study of that is beyond the scope of the present Letter.

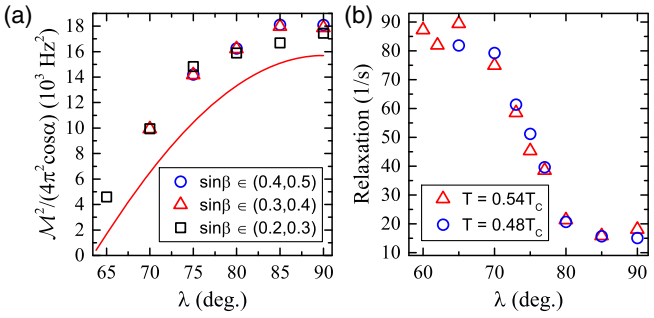

FIG. 4. Dependence of coherent precession on the magnetic field orientation λ. (a) The mass $\mathcal{M}$ of the pseudo-NG mode. Symbols represent ranges of $\sin\beta$ over which the mass has been averaged. The curve is the theoretical dependence for $\sin\beta = 0.45$ according to Eq. (4). For smaller β theoretical line goes lower. The measurements have been done with $H_{\rm rf}$ increasing from 0.16 μT to 0.48 μT as λ decreases from 90° to 65°, but are scaled in the plot with Eq. (4) to $H_{\rm rf} = 0.71$ μT, which coincides with the data in Fig. 3(c). Temperature is between $0.44T_c$ and $0.49T_c$. (b) The relaxation rate of magnon BEC at two temperatures.

The pseudo-NG mass $\mathcal{M}$ is plotted in Fig. 3 as a function of $H_{\rm rf}$, Ω_P (controlled by temperature T), and $\Delta\omega$, and in Fig. 4(a) as a function of λ. Experimental results for $\sin\beta > 0.4$ are in decent agreement with the theory given by Eq. (4). Discrepancies at small β in Figs. 3(c) and 4(a) are observed when $\Delta\omega$ is comparable to the linear cw NMR linewidth (≈300 Hz).

The relaxation rate τ^{-1} of magnon BEC, as a function of the field orientation λ, is plotted in Fig. 4(b). The slowest decay at the end of the relaxation is shown. It is measured by pulsed NMR, and the amplitude of the free induction decay signal is fitted by $\exp(-t/\tau)$. As expected, the magnon BEC shows maximum stability in the transverse field $\mathbf{H}\perp\hat{\mathbf{m}}$. With decreasing λ, the relaxation increases, and close to the critical angle λ_c, it is difficult to resolve the coherent precession.

Conclusions.—We have created a coherently precessing spin state in the polar phase of superfluid ^{3}He confined in Nafen. The coherent state is observed in cw and pulsed NMR when a large enough number of magnons is pumped by the rf field. This state has all the signatures of magnon BEC, supported by superfluid spin currents. In particular, its decay in the absence of pumping proceeds only via magnon loss. No dephasing of precession occurs, and coherence is preserved by spin supercurrents. The broken U(1) symmetry is manifested by the pseudo-Nambu-Goldstone collective mode of coherent precession [49,50]. We have measured this mode using resonant excitation and found that its frequency is in close agreement with the theory.

In the polar phase of superfluid ^{3}He, magnon BEC can be used as an excellent tool to study phenomena that are less prominent or inaccessible in other known topological superfluids. Remarkably, near the critical angle λ_c, the NG mode becomes nearly massless [see Eq. (4) and Fig. 4(a)] and also slow, as c in Eq. (3) decreases towards zero [48]. Thus, in the polar phase, the effective metric for the NG bosons can be controlled using the magnetic field profile. In particular, a black hole horizon can be modeled. Further applications of magnon BEC in the polar phase include studies of certain topological objects, like half-quantum vortices [43], probing a new type of quantum electrodynamics for "relativistic" fermions living in the vicinity of the Dirac line [51], and elucidating the interplay of the topology of the superfluid state with the disorder created by the confining matrix.

This work has been supported by the Academy of Finland (Projects No. 284594 and No. 298451) and by the European Research Council (ERC) under the European Union's Horizon 2020 research and innovation programme (Grant Agreement No. 694248). We used facilities of the Low Temperature Laboratory infrastructure of Aalto University. Some preliminary experiments have been performed at the Kapitza Institute and were supported by Basic Research Program of the Presidium of Russian Academy of Sciences and by Russian Foundation for Basic Research Grant No. 16-02-00349. S. A. acknowledges financial support from the Jenny and Antti Wihuri foundation.

*Present address: Department of Physics, Lancaster University, Lancaster LA1 4YB, United Kingdom.

[1] H. Fröhlich, Phys. Lett. **26A**, 402 (1968).
[2] Y. Kagan and L. A. Manakova, Phys. Lett. A **361**, 401 (2007).
[3] L. V. Butov, A. L. Ivanov, A. Imamoglu, P. B. Littlewood, A. A. Shashkin, V. T. Dolgopolov, K. L. Campman, and A. C. Gossard, Phys. Rev. Lett. **86**, 5608 (2001).
[4] J. Kasprzak, M. Richard, S. Kundermann, A. Baas, P. Jeambrun, J. M. J. Keeling, F. M. Marchetti, M. H. Szymańska, R. André, J. L. Staehli, V. Savona, P. B. Littlewood, B. Deveaud, and Le Si Dang, Nature (London) **443**, 409 (2006).
[5] J. Klaers, J. Schmitt, F. Vewinger, and M. Weitz, Nature (London) **468**, 545 (2010).
[6] L. A. Melnikovsky, Phys. Rev. B **84**, 024525 (2011).
[7] A. S. Borovik-Romanov, Y. M. Bunkov, V. V. Dmitriev, and Y. M. Mukharskiy, JETP Lett. **40**, 1033 (1984).
[8] A. S. Borovik-Romanov, Y. M. Bunkov, V. V. Dmitriev, Y. M. Mukharskiy, E. V. Poddyakova, and O. D. Timofeevskaya, Sov. Phys. JETP **69**, 542 (1989).
[9] I. A. Fomin, JETP Lett. **40**, 1037 (1984).
[10] Y. M. Bunkov, S. N. Fisher, A. M. Guénault, and G. R. Pickett, Phys. Rev. Lett. **69**, 3092 (1992).
[11] S. O. Demokritov, V. E. Demidov, O. Dzyapko, G. A. Melkov, A. A. Serga, B. Hillebrands, and A. N. Slavin, Nature (London) **443**, 430 (2006).
[12] Y. M. Bunkov and G. E. Volovik, Phys. Rev. Lett. **98**, 265302 (2007).
[13] S. Autti, Y. M. Bunkov, V. B. Eltsov, P. J. Heikkinen, J. J. Hosio, P. Hunger, M. Krusius, and G. E. Volovik, Phys. Rev. Lett. **108**, 145303 (2012).
[14] Y. M. Bunkov and G. E. Volovik, Int. Ser. Monogr. Phys. **156**, 253 (2013).
[15] O. Vainio, J. Ahokas, J. Järvinen, L. Lehtonen, S. Novotny, S. Sheludiakov, K.-A. Suominen, S. Vasiliev, D. Zvezdov, V. V. Khmelenko, and D. M. Lee, Phys. Rev. Lett. **114**, 125304 (2015).
[16] F. Fang, R. Olf, S. Wu, H. Kadau, and D. M. Stamper-Kurn, Phys. Rev. Lett. **116**, 095301 (2016).
[17] D. A. Bozhko, A. A. Serga, P. Clausen, V. I. Vasyuchka, F. Heussner, G. A. Melkov, A. Pomyalov, V. S. L'vov, and B. Hillebrands, Nat. Phys. **12**, 1057 (2016).
[18] A. S. Borovik-Romanov, Y. M. Bunkov, V. V. Dmitriev, and Y. M. Mukharskiy, JETP Lett. **45**, 124 (1987).
[19] A. S. Borovik-Romanov, Y. M. Bunkov, A. de Waard, V. V. Dmitriev, V. Makrotsieva, Y. M. Mukharskiy, and D. A. Sergatskov, JETP Lett. **47**, 478 (1988).
[20] A. S. Borovik-Romanov, Y. M. Bunkov, V. V. Dmitriev, Y. M. Mukharskiy, and D. A. Sergatskov, Phys. Rev. Lett. **62**, 1631 (1989).
[21] G. E. Volovik, JETP Lett. **87**, 639 (2008).
[22] I. A. Fomin, JETP Lett. **43**, 171 (1986).
[23] Y. M. Bunkov, V. V. Dmitriev, and Y. M. Mukharskiy, JETP Lett. **43**, 168 (1986).
[24] Y. Kondo, J. S. Korhonen, M. Krusius, V. V. Dmitriev, Y. M. Mukharsky, E. B. Sonin, and G. E. Volovik, Phys. Rev. Lett. **67**, 81 (1991).
[25] Y. Kondo, J. S. Korhonen, M. Krusius, V. V. Dmitriev, E. V. Thuneberg, and G. E. Volovik, Phys. Rev. Lett. **68**, 3331 (1992).
[26] V. B. Eltsov, R. de Graaf, M. Krusius, and D. E. Zmeev, J. Low Temp. Phys. **162**, 212 (2011).
[27] J. J. Hosio, V. B. Eltsov, P. J. Heikkinen, R. Hänninen, M. Krusius, and V. S. L'vov, Nat. Commun. **4**, 1614 (2013).
[28] J. T. Mäkinen and V. B. Eltsov, Phys. Rev. B **97**, 014527 (2018).
[29] P. J. Heikkinen, S. Autti, V. B. Eltsov, R. P. Haley, and V. V. Zavjalov, J. Low Temp. Phys. **175**, 681 (2014).
[30] V. V. Zavjalov, S. Autti, V. B. Eltsov, P. Heikkinen, and G. E. Volovik, Nat. Commun. **7**, 10294 (2016).
[31] S. Autti, P. J. Heikkinen, G. E. Volovik, V. V. Zavjalov, and V. B. Eltsov, Phys. Rev. B **97**, 014518 (2018).
[32] Y. M. Bunkov and G. E. Volovik, Europhys. Lett. **21**, 837 (1993).
[33] T. Sato, T. Kunimatsu, K. Izumina, A. Matsubara, M. Kubota, T. Mizusaki, and Y. M. Bunkov, Phys. Rev. Lett. **101**, 055301 (2008).
[34] V. V. Dmitriev, A. A. Senin, A. A. Soldatov, and A. N. Yudin, Phys. Rev. Lett. **115**, 165304 (2015).
[35] V. E. Asadchikov, R. S. Askhadullin, V. V. Volkov, V. V. Dmitriev, N. K. Kitaeva, P. N. Martynov, A. A. Osipov, A. A. Senin, A. A. Soldatov, D. I. Chekrygina, and A. N. Yudin, JETP Lett. **101**, 556 (2015).
[36] K. Aoyama and R. Ikeda, Phys. Rev. B **73**, 060504 (2006).
[37] T. T. Heikkilä and G. E. Volovik, New J. Phys. **17**, 093019 (2015).

[38] C. Fang, H. Weng, X. Dai, and Z. Fang, Chin. Phys. B **25**, 117106 (2016).
[39] R. Yu, Z. Fang, X. Dai, and H. Weng, Front. Phys. **12**, 127202 (2017).
[40] R. Blaauwgeers, M. Blazkova, M. Človečko, V. B. Eltsov, R. de Graaf, J. Hosio, M. Krusius, D. Schmoranzer, W. Schoepe, L. Skrbek, P. Skyba, R. E. Solntsev, and D. E. Zmeev, J. Low Temp. Phys. **146**, 537 (2007).
[41] E. V. Thuneberg, J. Low Temp. Phys. **122**, 657 (2001).
[42] P. J. Hakonen, M. Krusius, M. M. Salomaa, R. H. Salmelin, J. T. Simola, A. D. Gongadze, G. E. Vanchnadze, and G. A. Kharadze, J. Low Temp. Phys. **76**, 225 (1989).
[43] S. Autti, V. V. Dmitriev, J. T. Mäkinen, A. A. Soldatov, G. E. Volovik, A. N. Yudin, V. V. Zavjalov, and V. B. Eltsov, Phys. Rev. Lett. **117**, 255301 (2016).
[44] V. V. Dmitriev, A. A. Soldatov, and A. N. Yudin, Phys. Rev. Lett. **120**, 075301 (2018).
[45] I. A. Fomin, JETP Lett. **39**, 466 (1984).
[46] V. V. Dmitriev, V. V. Zavjalov, and D. Y. Zmeev, J. Low Temp. Phys. **138**, 765 (2005).
[47] M. Človečko, E. Gažo, M. Kupka, and P. Skyba, Phys. Rev. Lett. **100**, 155301 (2008).
[48] J. Nissinen and G. E. Volovik, Pis'ma Zh. Eksp. Teor. Fiz. **106**, 220 (2017) [JETP Lett. **106**, 234 (2017)].
[49] H. Watanabe, T. Brauner, and H. Murayama, Phys. Rev. Lett. **111**, 021601 (2013).
[50] M. Nitta and D. A. Takahashi, Phys. Rev. D **91**, 025018 (2015).
[51] B. Lian, C. Vafa, F. Vafa, and S.-C. Zhang, Phys. Rev. B **95**, 094512 (2017).